

Constraints on bosonic dark matter from ultralow-field nuclear magnetic resonance

Antoine Garcon^{a,b}, John W. Blanchard^{b,*}, Gary P. Centers^{a,b}, Nataniel L. Figueroa^{a,b}, Peter W. Graham^c, Derek F. Jackson Kimball^d, Surjeet Rajendran^e, Alexander O. Sushkov^f, Yevgeny V. Stadnik^{a,b}, Arne Wickenbrock^{a,b}, Teng Wu^{a,b}, Dmitry Budker^{a,b,e,g}

^a*Johannes Gutenberg-Universität, Mainz 55128, Germany*

^b*Helmholtz-Institut Mainz, 55128 Mainz, Germany*

^c*Department of Physics, Stanford Institute for Theoretical Physics, Stanford University, California 94305, USA*

^d*Department of Physics, California State University East Bay, Hayward, California 94542-3084, USA*

^e*Department of Physics, University of California, Berkeley, CA 94720-7300, USA*

^f*Department of Physics, Boston University, Boston, Massachusetts 02215, USA*

^g*Nuclear Science Division, Lawrence Berkeley National Laboratory, Berkeley, CA 94720, USA*

Abstract

The nature of dark matter, the invisible substance making up over 80% of the matter in the Universe, is one of the most fundamental mysteries of modern physics. Ultralight bosons such as axions, axion-like particles or dark photons could make up most of the dark matter. Couplings between such bosons and nuclear spins may enable their direct detection via nuclear magnetic resonance (NMR) spectroscopy: as nuclear spins move through the galactic dark-matter halo, they couple to dark-matter and behave as if they were in an oscillating magnetic field, generating a dark-matter-driven NMR signal. As part of the Cosmic Axion Spin Precession Experiment (CASPER), an NMR-based dark-matter search, we use ultralow-field NMR to probe the axion-fermion “wind” coupling and dark-photon couplings to nuclear spins. No dark matter signal was detected above background, establishing new experimental bounds for dark-matter bosons with masses ranging from 1.8×10^{-16} to 7.8×10^{-14} eV.

1. INTRODUCTION

1.1. Ultralight bosonic dark matter

The nature of dark matter, the invisible substance that makes up over 80% of the matter in the universe [1], is one of the most intriguing mysteries of modern physics [2]. Elucidating the nature of dark matter will profoundly impact our understanding of cosmology, astrophysics, and particle physics, providing insights into the evolution of the Universe and potentially uncovering new physical laws and fundamental forces beyond the Standard Model. While the observational evidence for dark matter is derived from its gravitational effects at the galactic scale and larger, the key to solving the mystery of its nature lies in directly measuring non-gravitational interactions of dark matter with Standard Model particles and fields.

To date, experimental efforts to directly detect dark matter have largely focused on Weakly Interacting Massive Particles (WIMPs), with masses between 10 and 1000 GeV [3, 4]. Despite considerable efforts, there have been no conclusive signs of WIMP interactions with ordinary matter. The absence of evidence for WIMPs has reinvigorated efforts to search for ultralight bosonic fields, another class of theoretically well-motivated dark matter candidates [5], composed of bosons with masses

smaller than a few eV. A wide variety of theories predict new spin-0 bosons such as axions and axion-like particles (ALPs) as well as spin-1 bosons such as dark photons [1, 6]. Their existence may help to answer other open questions in particle physics such as why the strong force respects the combined charge-conjugation and parity-inversion (CP) symmetry to such a high degree [7], the relative weakness of the gravitational interaction [8], and how to unify the theories of quantum mechanics and general relativity [9].

Bosonic fields can be detected through their interactions with Standard Model particles. Most experiments searching for bosonic fields seek to detect photons created by the conversion of these bosons in strong electromagnetic fields via the Primakoff effect [10–16]. Another method to search for dark-matter bosonic fields was recently proposed: dark-matter-driven spin-precession [17–19], detected via nuclear magnetic resonance (NMR) techniques [18–22]. These concepts were recently applied to data measuring the permanent electric dipole moment (EDM) of the neutron and successfully constrained ALP dark matter with masses $\lesssim 10^{-17}$ eV [22].

The Cosmic Axion Spin Precession Experiment (CASPER) is a multi-faceted research program using NMR techniques to search for dark-matter-driven spin precession [18]. Efforts within this program utilizing zero- to ultralow-field (ZULF) NMR spectroscopy [23] are collectively referred to as CASPER-ZULF. We report here experimental results from a CASPER-ZULF search for

*Corresponding author: blanchard@uni-mainz.de

ultralight bosonic dark-matter fields, probing bosons with masses ranging from 1.8×10^{-16} to 7.8×10^{-14} eV (corresponding to Compton frequencies ranging from ~ 45 mHz to 19 Hz).

In the following section, we explain how dark-matter bosonic fields, in particular axion, ALP and dark-photon fields, can be detected by examining ZULF NMR spectra. The subsequent sections describe the measurement scheme and the data processing techniques employed during this search. Finally we present new laboratory results for bosonic dark matter, complementing astrophysical constraints obtained from supernovae 1987A¹ [26].

2. RESULTS

2.1. Dark-matter field properties

If dark matter predominantly consists of particles with masses $m_{\text{DM}} \lesssim 10$ eV, making up the totality of the average local dark-matter density, then they must be bosons with a large mode occupation number. It would be impossible for fermions with such low masses to account for the observed galactic dark matter density, since the Pauli exclusion principle prevents them from having the required mode occupation.

In this scenario, axion and ALP bosonic dark matter is well described by a classical field $a(t)$, oscillating at the Compton frequency ($\omega_{\text{DM}} \approx m_{\text{DM}}c^2/\hbar$) [27–29]:

$$a(t) \approx a_0 \cos(\omega_{\text{DM}}t), \quad (1)$$

where c is the velocity of light, \hbar is the reduced Planck constant and a_0 is the amplitude of the bosonic field.

The temporal coherence of the bosonic field is limited by the relative motion of the Earth through random spatial fluctuations of the field. The characteristic coherence time τ_{DM} , during which the bosonic dark-matter fields remains phase coherent, corresponds to $\sim 10^6$ periods of oscillation of the fields [18].

The amplitude a_0 can be estimated by assuming that the field energy density constitutes the totality of the average local dark-matter energy density ($\rho_{\text{DM}} \approx 0.4$ GeV/cm³ [30]). Then a_0 is related to the dark-matter density through:

$$\rho_{\text{DM}} = \frac{1}{2} \frac{c^2}{\hbar^2} m_{\text{DM}}^2 \langle a_0 \rangle^2. \quad (2)$$

We note that a_0 is expected to fluctuate with relative amplitude of order one due to self-interference of the field. For simplicity we assume that $a_0 = \langle a_0 \rangle$.

¹We note that the constraints based on SN1987A data continue to be reexamined; see e.g. Refs. [24, 25].

2.2. Dark-matter couplings to nuclear spins

CASPER-Wind is sensitive to any field such that its interaction with nuclear spins can be written in the form:

$$\mathcal{H}_{\text{DM}} = -\hbar g_{\text{N}} \mathbf{I}_{\text{N}} \cdot \mathbf{D}, \quad (3)$$

where g_{N} is a coupling constant that parametrizes the coupling of the effective field, \mathbf{D} , to nuclear spins represented by the operator \mathbf{I}_{N} . In analogy with the Zeeman interaction, $\mathcal{H}_{\text{Zeeman}} = -\hbar \gamma_{\text{N}} \mathbf{I}_{\text{N}} \cdot \mathbf{B}$, such an effective field \mathbf{D} may be thought of as a pseudo-magnetic field interacting with nuclear spins, where the nuclear gyromagnetic ratio, γ_{N} , is replaced by the coupling constant, g_{N} .

For clarity, we focus this discussion on the the so-called “axion wind interaction” with effective field $\mathbf{D}_{\text{wind}} = -\nabla a(\mathbf{r}, t)$ and coupling constant g_{aNN} . A number of other possible couplings between nuclear spins and bosonic dark matter fields take a form similar to Eq. (3). These include couplings to the “dark” electric (with coupling g_{dEDM} and effective field \mathbf{D}_{dEDM}) and magnetic (with coupling g_{dMDM} and effective field \mathbf{D}_{dMDM}) fields mediated by spin-1 bosons such as dark photons [5, 31] or a quadratic “wind” coupling to an ALP field (with coupling g_{quad} and effective field \mathbf{D}_{quad}) [32]. These are discussed further in the Materials and Methods section.

As the Earth orbits around the Sun (itself moving towards the Cygnus constellation at velocity, \mathbf{v} , comparable to the local galactic virial velocity $\sim 10^{-3}c$), it moves through the galactic dark-matter halo and an interaction between axions and ALPs with a given nucleon N , can arise. Assuming that ALPs make up all of the dark matter energy density, ρ_{DM} , and that the dominant interaction with nucleon spins is linear in $\nabla a(\mathbf{r}, t)$, Eqs. (1) and (2) can be used to write the effective field as

$$\mathbf{D}_{\text{wind}}(t) = -\sqrt{2\hbar c \rho_{\text{DM}}} \sin(\omega_{\text{DM}}t) \mathbf{v}. \quad (4)$$

Then, given the local galactic virial velocity, \mathbf{v} , only two free parameters remain in the Hamiltonian in Eq. (3): the coupling constant, g_{aNN} , and the field’s oscillation frequency, ω_{DM} , fixed by the boson mass. A CASPER search consists of probing this parameter space over a bosonic mass range defined by the bandwidth of the experiment. In order to calibrate the experiment, we apply known magnetic fields and the experiment’s sensitivity to magnetic fields directly translates to sensitivity to the coupling constant. If no ALP field is detected, upper bounds on the coupling constant can be determined based on the overall sensitivity of the experiment.

2.3. Dark-matter signatures in zero- to ultralow-field NMR

The results presented in this work were obtained by applying techniques of ZULF NMR (see Materials and Methods Sec. 4.1, a review of ZULF NMR can be found in Ref. [23]). The sample – ¹³C-formic acid,

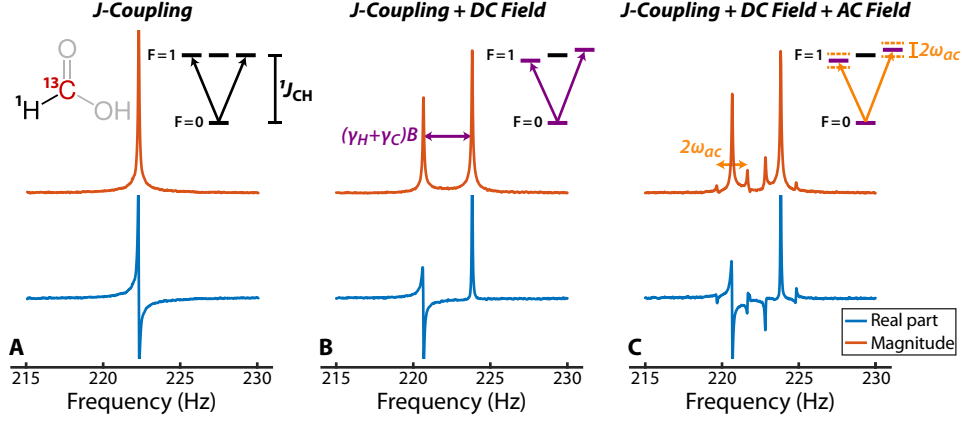


Figure 1: Nuclear spin energy levels and NMR spectra of ^{13}C -formic acid measured in three different field conditions. **(a)** At zero magnetic field, the $F = 1$ levels are degenerate, resulting in a spectrum exhibiting a single peak at the J -coupling frequency. **(b)** In the presence of a DC-magnetic field $B_z \approx 50$ nT, the $m_F = \pm 1$ degeneracy is broken. The spectrum exhibits two split J -resonances. The splitting is equal to $\hbar m_F B_z (\gamma_C + \gamma_H)$. The asymmetry of the resonances is due to the influence of the applied field on the response characteristics of the atomic magnetometer. **(c)** The addition of an oscillating magnetic field along B_z modulates the $m_F = \pm 1$ energy levels, resulting in sidebands located at $J/2\pi \pm B_z(\gamma_C + \gamma_H)/2 \pm \omega_{AC}$ with amplitude proportional to the modulation index: $A_s \propto B_{AC}(\gamma_C + \gamma_H)/2\omega_{AC}$.

effectively a two-spin ^1H - ^{13}C system – is pre-polarized in a 1.8 T permanent magnet and pneumatically shuttled to a magnetically-shielded environment for magnetization evolution and detection.

The spin Hamiltonian describing the system is

$$\mathcal{H} = \hbar J_{\text{CH}} \mathbf{I} \cdot \mathbf{S} - \hbar (\gamma_{\text{H}} \mathbf{I} + \gamma_{\text{C}} \mathbf{S}) \cdot \mathbf{B} + \hbar \left(g_{\text{app}} \mathbf{I} - \frac{1}{3} g_{\text{ann}} \mathbf{S} \right) \cdot \mathbf{D}_{\text{wind}}(t), \quad (5)$$

where the electron-mediated spin-spin coupling $J_{\text{CH}}/2\pi \approx 221$ Hz for formic acid and \mathbf{I} and \mathbf{S} are the nuclear-spin operators for ^1H and ^{13}C , respectively. Additionally, γ_{H} and γ_{C} are the gyromagnetic ratios of the ^1H and ^{13}C spins, \mathbf{B} is an applied magnetic field, g_{app} is the ALP-proton coupling strength, and g_{ann} is the ALP-neutron coupling strength. We assume $g_{\text{app}} = g_{\text{ann}} = g_{\text{aNN}}$ [22].

In the absence of external fields ($\mathbf{B} = \mathbf{D}_{\text{wind}}(t) = 0$), the nuclear spin energy eigenstates are a singlet with total angular momentum $F = 0$ and three degenerate triplet states with $F = 1$, separated by $\hbar J_{\text{CH}}$. The observable in our experiment is the y magnetization, leading to selection rules $\Delta F = 0, \pm 1$ and $\Delta m_F = \pm 1$, as in Ref. [33]. The zero-field spectrum thus consists of a single Lorentzian located at $J_{\text{CH}}/2\pi \approx 221$ Hz, as shown in Fig. 1(a).

In the presence of a static magnetic field, $\mathbf{B} = B_z \hat{e}_z$, applied along z , the $m_F = 0$ states are unaffected, while the $m_F = \pm 1$ triplet states' degeneracy is lifted. The corresponding spectrum exhibits two peaks at $J_{\text{CH}}/2\pi \pm B_z(\gamma_{\text{H}} + \gamma_{\text{C}})/2\pi$, as shown in Fig. 1(b).

So long as $|J_{\text{CH}}| \gg |\gamma_{\text{H}} B| \gg |g_{\text{aNN}} D_{\text{wind}}|$ the $m_F = 0$ states are unaffected, and the $m_F = \pm 1$ states are shifted

by

$$\Delta E(m_F = \pm 1)(t) = \mp \frac{\hbar}{2} B_z (\gamma_{\text{H}} + \gamma_{\text{C}}) \pm \frac{\hbar}{2} \frac{2}{3} g_{\text{aNN}} D_z(t), \quad (6)$$

where $D_z(t)$ is the projection of $\mathbf{D}_{\text{wind}}(t)$ along the axis of the applied magnetic field. The time dependence of $\mathbf{D}_{\text{wind}}(t)$ leads to an oscillatory modulation of the $m_F = \pm 1$ energy levels, giving rise to sidebands around the J -coupling doublet as shown in Fig. 1(c). The sidebands are separated from the carrier peaks by $\pm \omega_{\text{DM}}/2\pi$ and have an amplitude proportional to the modulation index ($g_{\text{aNN}}/\omega_{\text{DM}}$).

Dark-matter fields with sufficiently strong coupling to nuclear spins can then be detected by searching for frequency-modulation-induced sidebands in the well-defined ZULF NMR spectrum of formic acid.

2.4. Coherent averaging

The expected dark matter coherence time (~ 14 hours for a particle with 19 Hz Compton frequency) is much longer than the nuclear spin coherence time in ^{13}C -formic acid (~ 10 s). Taking advantage of this mismatch, we introduce the post-processing phase-cycling technique shown in Fig. 2 (see Materials and Methods Sec. 4.3), which consists of incrementally phase-shifting the transient spectra and subsequently averaging them together. If the phase increment matches the phase accumulated by the oscillating field between each transient acquisition, the sidebands add constructively. This allows coherent averaging of the complex spectra, such that the signal-to-noise ratio scales as $N^{1/2}$, where N is the number of transients. Because the dark-matter Compton frequency is unknown, it is necessary to repeat this

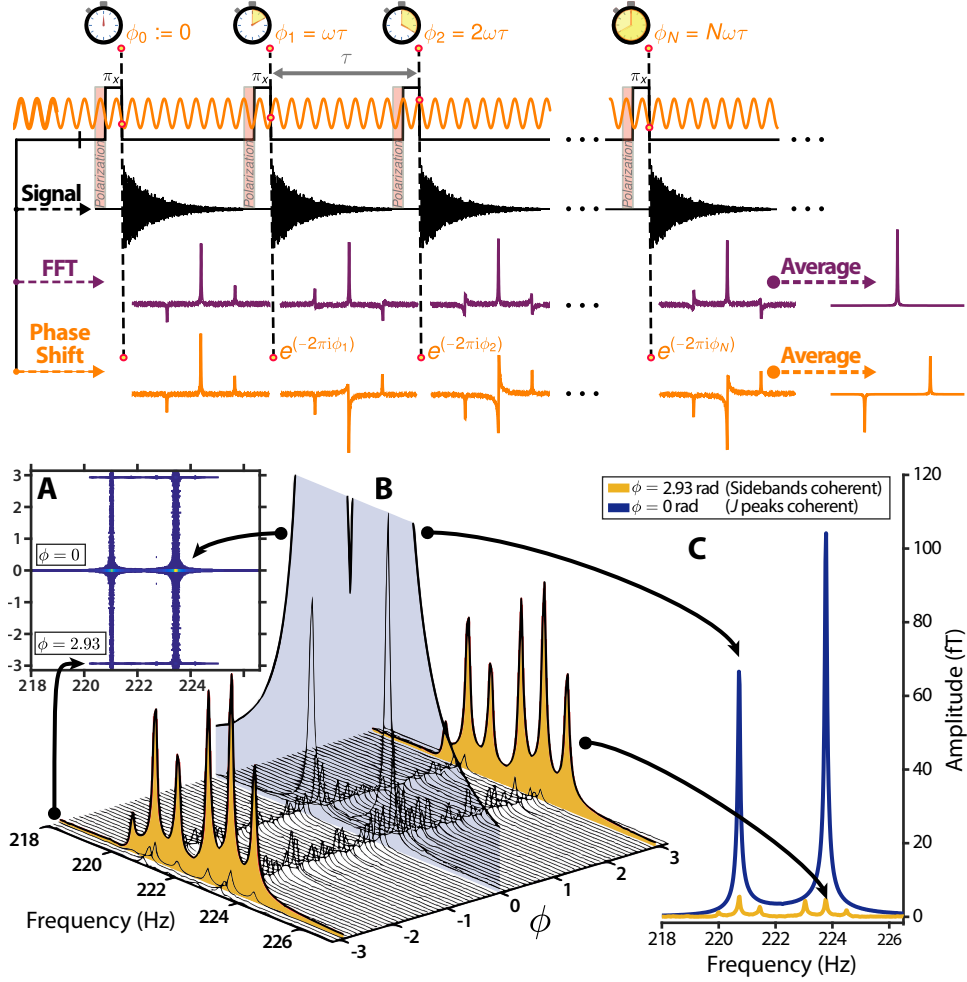


Figure 2: **Top:** signal acquisition scheme with simulated spectra. After polarization, each transient acquisition starts following a magnetic π -pulse (corresponding to a 180 degrees flip of the ^{13}C spin along any direction). The external AC-magnetic field's phase varies between transient acquisitions (orange). As a result, the sidebands generally possess different phases in each transient spectrum. Averaging the transients yields a spectrum in which the sidebands are destructively averaged out (purple). Shifting each transient by a phase equal to the external field's accumulated phase restores the sidebands' phase coherence, yielding a spectrum with high signal-to-noise ratio sidebands (orange). For clarity, only one of the two Zeeman-split J -coupling peaks and its two sidebands are shown. **Bottom:** result of the phase-shifting procedure for actual data. (a) Transients are averaged using 2001 phase increments and stacked into a two-dimensional plot. (b) Side view of (a), sidebands are rescaled by a factor 10 for clarity. (c) Averaging with $\phi = 0$ rad corresponds to averaging the transients without phase-shift; sidebands are averaged out and carrier peaks appear with maximum amplitude. When the optimal phase (for $\omega/2\pi = 0.73$ Hz, $\phi = 2.93$ rad) is approached, sidebands appear. These spectra were acquired in an experiment during which the AC-field frequency and amplitude were set to 0.73 Hz and 0.24 nT. Transient acquisitions of 30 s were repeated 850 times with a time interval between each transient of $\tau = 61$ s.

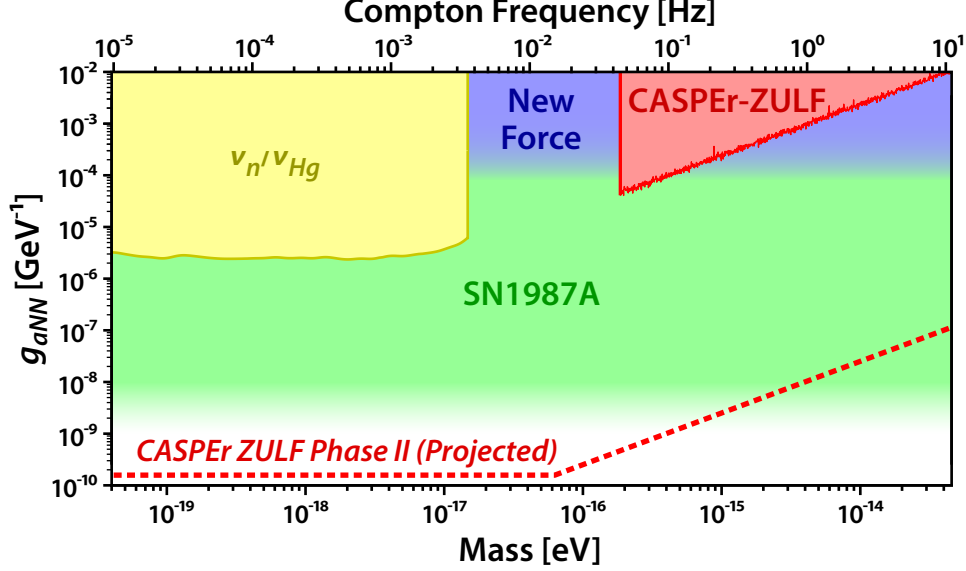


Figure 3: ALP-nucleon linear coupling parameter space. The CASPER-ZULF region is excluded by this work (90% confidence level) using a thermally polarized sample (data averaged over 850 transient acquisitions of 30 s each). The “New Force” region is excluded by searches for new spin-dependent forces [34]. The SN1987A region represents existing limits from supernova SN1987A cooling [26, 35]. The ν_n/ν_{Hg} region is excluded by measurements of the ratio of neutron and ^{199}Hg Larmor precession frequencies [22]. The dashed line corresponds to the sensitivity of a planned second phase of CASPER-ZULF, with a projected $\sim 10^5$ factor increase in sensitivity and the bandwidth extended towards lower frequencies by using a comagnetometer technique [36] and longer integration times.

operation for a large number of different phase increments (at least many as the number of transient acquisitions).

2.5. Calibration

The energy shifts produced by $D_z(t)$ [Eq. (6)] are equivalent to those produced by a real magnetic field with amplitude

$$B_{\text{wind}}(t) = \frac{2}{3} \frac{g_{aNN}}{\gamma_H + \gamma_C} \cdot D_z(t) \propto \frac{g_{aNN}}{\gamma_H + \gamma_C} \sqrt{\rho_{\text{DM}}} \sin(\omega_{\text{DM}} t) \mathbf{v} \cdot \hat{\mathbf{e}}_z. \quad (7)$$

Similar relationships for dark-photon and quadratic-wind couplings are provided in the Materials and Methods section.

Based on Eq. (7), the sensitivity of the experiment to dark matter was calibrated by applying a real oscillating magnetic field of known amplitude and frequency and measuring the amplitude of the resulting sidebands in the coherently averaged spectrum. Further details are provided in the Supplementary Materials.

2.6. Search and analysis

The dark matter search data were acquired and processed as described above, but without a calibration AC-magnetic field applied.

For each Compton frequency, the appropriate phase increment is computed, which identifies the corresponding coherently averaged spectrum to be analyzed. The noise in the spectrum defines a detection threshold at the 90%

confidence level (further details in S7 of the Supplementary Materials). When the signal amplitude at the given frequency is below the threshold, we set limits on the dark matter couplings to nuclear spins at levels determined by the calibration and effective-field conversion factors (see Materials and Methods Sec. 4.2). If the signal is above the threshold, a more stringent analysis is performed by fitting the coherently averaged spectrum to a four-sideband model. When the fit rules out detection, the threshold level is again used to set limits.

In case of an apparent detection, further repeat measurements would need to be performed to confirm that the signal is persistent and exhibits expected sidereal and annual variations.

2.7. CASPER-ZULF search results: constraints on bosonic dark matter

The results of the CASPER-ZULF search for axionlike particles are given in Fig. 3. The frequencies presenting sharp losses in sensitivities at 0.21, 1.69, and 2.16 Hz were the ones for which the nearest optimal phase increment was close to zero, thus presenting maximal-amplitude J -coupling peaks, raising the detection threshold (see discussion in Sec. S3 of the Supplementary Materials). The red-shaded area labeled “CASPER-ZULF” corresponds to upper bounds on nuclear-spin couplings to dark matter consisting of ALPs at the 90% confidence level. This represents our current sensitivity limitation after 850 30-second transient acquisitions using samples thermally polarized at ~ 1.8 T. The “CASPER-ZULF Phase II” line corresponds to the projected sensitivity of a future

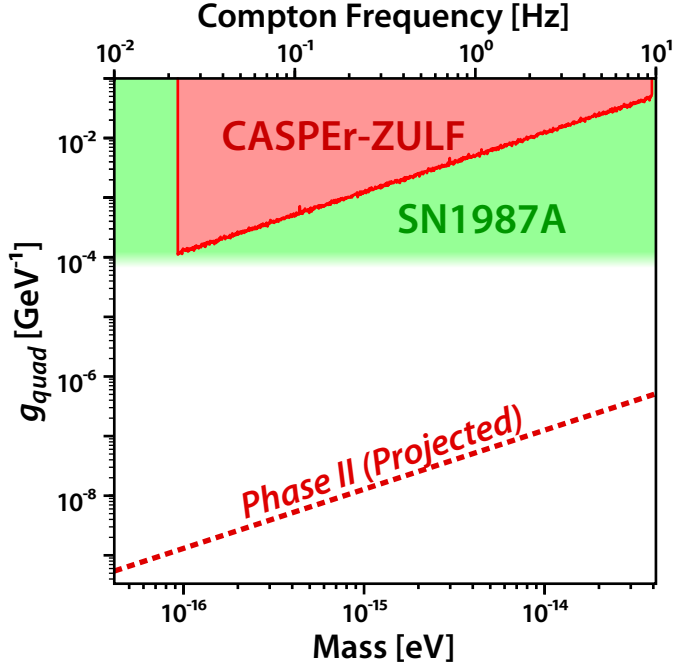


Figure 4: ALP-nucleon quadratic coupling parameter space. The CASPER-ZULF region is excluded by this work (90% confidence level) using a thermally polarized sample (data averaged over 850 transient acquisitions of 30 s each). Other regions of this figure are defined in the caption of Fig. 3.

iteration of this work that will use a more sensitive magnetometry scheme to measure a larger sample with enhanced (non-equilibrium) nuclear spin polarization.

Figures 4 and 5 show the search results for the ALP quadratic interaction and dark photon interactions, respectively. No signal consistent with axion, ALP or dark-photon fields have been observed in the red-shaded areas. The two different limits given in Fig. 5 were obtained using the same data set but analyzed by assuming two orthogonal initial polarizations of the dark-photon field (see S10 of the Supplementary Materials).

In all cases, the search bandwidth was limited from below by the finite linewidth of the J -resonance peaks, preventing to resolve sidebands at frequencies lower than 45 mHz. Due to the finite coherence time of the dark-matter fields (corresponding to $\sim 10^6$ oscillations), the bandwidth's upper limit (19 Hz), is the highest frequency which can be coherently averaged after 14 hours of integration time. The sensitivity fall off is due to the sidebands' amplitude scaling as the modulation index. Further details are given in S6 and S9 of the Supplementary Materials.

3. DISCUSSION

This work constitutes demonstration of a dark-matter search utilizing NMR techniques with a coupled heteronuclear spin system. The results provide new laboratory-based upper bounds for bosonic dark matter with masses

ranging from 1.86×10^{-16} to 7.85×10^{-14} eV, complementing astrophysical bounds obtained from supernova SN1987A [26, 35].

Our data analysis provides a method to perform coherent averaging of the bosonic-field-induced transient signals. This method should prove useful for other experiments seeking to measure external fields of unknown frequency using a detector with a comparatively short coherence time. Conveniently, this phase-cycling approach also suppresses the carrier-frequency signals, which would otherwise increase the detection threshold via spectral leakage. As this method is applied during post-processing, it does not require modification of the experiments provided that the data to be analyzed have been time stamped.

3.1. Phase II Sensitivity Improvements

In order to search a greater region of the bosonic dark-matter parameter spaces, several sensitivity-enhancing improvements are planned for the next phase of the experiment. In this work, nuclear spin polarization was achieved by allowing the sample to equilibrate in a 1.8-T permanent magnet, which yields a ^1H polarization $\lesssim 10^{-5}$. For the next phase of the experiment, a substantial sensitivity improvement can be obtained by using so-called “hyperpolarization” methods to achieve much higher, non-equilibrium nuclear-spin polarization. Current efforts are focused on the implementation of non-hydrogenative parahydrogen-induced polarization (NH-PHIP)² [38]. Signal enhancement via NH-PHIP has been demonstrated at zero field [39] and after optimization is expected to increase nuclear spin polarization levels to at least 1%. Because parahydrogen can be flowed continuously into the sample, a steady-state polarization enhancement can be achieved [40], improving the experimental duty cycle. Combining continuous NH-PHIP with a feedback system to produce a self-oscillating nuclear spin resonator [41] could conceivably offer further improvement and simplify data analysis.

Additional sensitivity enhancement will be provided by magnetometer improvements and use of a larger sample. In the experiments reported here, only about 50 μL of the sample contributed to the signal, which was detected from below with an atomic magnetometer with a noise floor around $10 \text{ fT}/\sqrt{\text{Hz}}$. With a larger ($\gtrsim 1 \text{ mL}$) sample hyperpolarized via NH-PHIP detected via a gradiometric magnetometer array with optimized geometry and sensitivity below $1 \text{ fT}/\sqrt{\text{Hz}}$, we anticipate an improvement by $\gtrsim 10^5$ relative to the results presented here.

Future experiments will be carried out with increased integration time. We recall that the bosonic dark-matter fields are coherent for a time τ_{DM} on the order of

²Non-hydrogenative parahydrogen-induced polarization methods are often referred to with the acronym SABRE, for Signal Amplification by Reversible Exchange of parahydrogen.

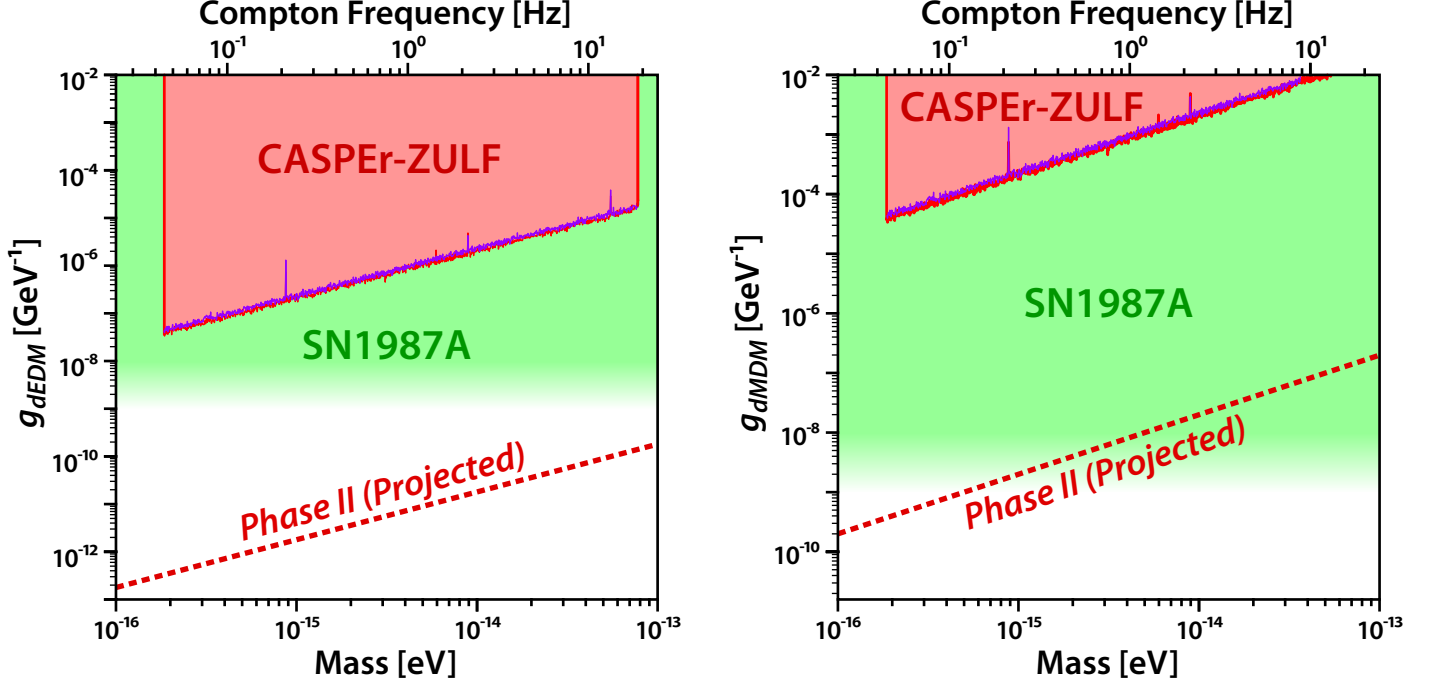


Figure 5: Left: dark photon-nucleon dEDM coupling parameter space. The SN1987A region represents existing limits for ALPs from supernova SN1987A cooling [26, 35] adjusted to constrain dark photons as discussed in Ref. [37]. Right: dark photon-nucleon dMDM coupling parameter space. The CASPER-ZULF regions are excluded by this work (90% confidence level) using a thermally polarized sample (data averaged over 850 transient acquisitions of 30 s each). The red and purple lines correspond to the case where the dark-photon field polarization is along the \hat{e}_1 and \hat{e}_3 axes of the non-rotating Celestial frame, respectively (see section S10 of the Supplementary Materials). The dashed lines correspond to the sensitivity of a planned second phase of CASPER-ZULF, with a projected $\sim 10^5$ factor increase in sensitivity.

10^6 periods of oscillation. The phase-cycling procedure depicted in Fig. 2 is valid for data sets with total time less than τ_{DM} . For integration times longer than the coherence time of the bosonic field $T_{\text{tot}} > \tau_{DM}$, the data sets have to be coherently averaged in sets of duration τ_{DM} using the phase-cycling procedure. This yields T_{tot}/τ_{DM} sets of coherently averaged data. To profit from longer integration time and further increase the SNR, these sets can be incoherently averaged by averaging their PSDs, yielding an overall SNR scaling as $(T_{\text{tot}}\tau_{DM})^{1/4}$ (see Supplementary Materials in Ref. [18]).

3.2. Complementary Searches

In order to increase the bandwidth of the experiment (see Supplementary Materials S9), we propose complementary measurement procedures. As the amplitude of the sidebands scales as $1/\omega_{DM}$, the sensitivity of the experiment decreases for higher frequencies. To probe frequencies ranging from ~ 20 to 500 Hz (corresponding to bosonic masses of $\sim 8 \times 10^{-14}$ to 2×10^{-12} eV), it was shown in Ref. [42] that a resonant detection method will be more sensitive than the current frequency-modulation-induced sidebands measurement scheme. Resonant AC fields can induce phase shifts in the J -coupling peaks [43]; cosmic fields can induce the same effect. By gradually varying the magnitude of a leading magnetic field, one can tune the splitting of the J -coupling multiplets to match the dark-matter field frequency. Such a resonance would manifest

itself by shifting the phase of the J -coupling peak.

For frequencies below ~ 45 mHz (corresponding to bosonic masses $\lesssim 2 \times 10^{-16}$ eV), the sidebands are located inside of the J -coupling peaks and the experimental sensitivity drops rapidly. This represents the lower limit of the bandwidth accessible by the frequency-modulation-induced sidebands measurement scheme presented in this work. To probe down to arbitrarily low frequencies, another measurement scheme has been implemented based on a single-component liquid-state nuclear-spin comagnetometer [44]. Further details and results of this scheme are presented elsewhere [36].

4. MATERIALS AND METHODS

4.1. Experimental parameters

The experimental setup used in this experiment is the one described in Ref. [45]. Additional descriptions of similar ZULF NMR setups can be found in Refs [46]. A schematic of the apparatus is given in Fig. S1 of the Supplementary Materials.

The NMR sample consists of ~ 100 μL of liquid ^{13}C -formic acid ($^{13}\text{CHOOH}$) obtained from ISOTEC Stable Isotopes (Millipore Sigma), degassed by several freeze-pump-thaw cycles under vacuum, and flame-sealed in a standard 5 mm glass NMR tube.

The sample is thermally polarized for ~ 30 s in a 1.8-T permanent magnet, after which the NMR tube is pneumatically shuttled into the zero-field region. After the guiding magnetic field is turned off, a magnetic pulse (corresponding to a π rotation of the ^{13}C spin) is applied to initiate magnetization evolution.

Following each transient acquisition, the sample is shuttled back into the polarizing magnet and the experiment is repeated. In order

to increase the SNR, the transient signals are averaged using the phase-cycling technique described in Sec. 4.3.

4.2. Bosonic dark-matter effective fields

In the case of the ALP-wind linear coupling, the field acting on the ^1H - ^{13}C spins induces an energy shift equal to the one produced by a magnetic field with amplitude

$$B_{\text{ALP},z}^{\text{eff}}(t) = -\frac{2}{3} \frac{g_{\text{aNN}}}{\gamma_{\text{H}} + \gamma_{\text{C}}} \sqrt{2\hbar c \rho_{\text{DM}}} \times \sin(\omega_{\text{DM}} t - \mathbf{k} \cdot \mathbf{r} + \phi) \mathbf{v} \cdot \hat{\mathbf{e}}_z, \quad (8)$$

where $\omega_{\text{DM}} \approx m_{\text{DM}} c^2 / \hbar$ is the ALP Compton frequency, $\mathbf{k} \approx m_{\text{DM}} \mathbf{v} / \hbar$ is the wave-vector (\mathbf{v} is the relative velocity), m_{DM} is the rest mass of the ALP, ϕ is an unknown phase, and $\hat{\mathbf{e}}_z$ is the axis along which the leading DC-magnetic field is applied.

It is theoretically possible that interaction of nuclear spins with ∇a can be suppressed [32, 47], in which case the dominant axion wind interaction, referred to as the quadratic wind coupling, is related to ∇a^2 . In the case of the ALP-wind quadratic coupling the equivalent magnetic field amplitude is:

$$B_{\text{quad},z}^{\text{eff}}(t) = -\frac{4}{3} \hbar c^2 \frac{g_{\text{quad}}^2}{\gamma_{\text{H}} + \gamma_{\text{C}}} \frac{\rho_{\text{DM}}}{\omega_{\text{DM}}} \times \sin(2\omega_{\text{DM}} t - 2\mathbf{k} \cdot \mathbf{r} + \phi) \mathbf{v} \cdot \hat{\mathbf{e}}_z. \quad (9)$$

where g_{quad} , having dimensions of inverse energy, parameterizes the ALP quadratic coupling strength to nuclear spins.

There are two possible interactions of dark photons with nuclear spins that can be detected with CASPER-ZULF: the coupling of the dark electric field to the dark electric dipole moment (dEDM) and the coupling of the dark magnetic field to the dark magnetic dipole moment (dMDM). The equivalent magnetic field amplitudes are:

$$B_{\text{dEDM}}^{\text{eff}}(t) = \frac{2}{3} \frac{g_{\text{dEDM}}}{\gamma_{\text{C}} + \gamma_{\text{H}}} \sqrt{2\hbar c^3 \rho_{\text{DM}}} \times \cos(\omega_{\text{DM}} t + \phi) \boldsymbol{\epsilon} \cdot \hat{\mathbf{e}}_z, \quad (10)$$

and

$$B_{\text{dMDM}}^{\text{eff}}(t) = \frac{2}{3} \frac{g_{\text{dMDM}}}{\gamma_{\text{C}} + \gamma_{\text{H}}} \frac{v}{c} \sqrt{2\hbar c^3 \rho_{\text{DM}}} \times \cos(\omega_{\text{DM}} t + \phi) \boldsymbol{\epsilon} \cdot \hat{\mathbf{e}}_z, \quad (11)$$

with coupling constants g_{dEDM} and g_{dMDM} (having dimensions of inverse energy) and dark photon field polarization $\boldsymbol{\epsilon}$.

The experimental sensitivity to real magnetic fields then directly translates to sensitivity to the coupling constants g_{aNN} , g_{quad} , g_{dEDM} , and g_{dMDM} . Inverting equations (8)–(11) yields the corresponding conversion factors from magnetic field to the dark-matter coupling constants:

$$\delta g_{\text{aNN}}(\omega) \approx \left[1.3 \times 10^8 \frac{\text{GeV}^{-1}}{\text{T}} \right] \delta B(\omega), \quad (12)$$

$$\delta g_{\text{quad}}(\omega) \approx \left[190 \frac{\text{GeV}^{-1}}{\sqrt{\text{T}} \sqrt{\text{rad/s}}} \right] \sqrt{\omega \cdot \delta B(\omega)}, \quad (13)$$

$$\delta g_{\text{dEDM}}(\omega) \approx \left[1.3 \times 10^5 \frac{\text{GeV}^{-1}}{\text{T}} \right] \delta B(\omega), \quad (14)$$

$$\delta g_{\text{dMDM}}(\omega) \approx \left[1.3 \times 10^8 \frac{\text{GeV}^{-1}}{\text{T}} \right] \delta B(\omega). \quad (15)$$

Here we have used $\gamma_{\text{C}}/2\pi = 10.70 \text{ MHz} \cdot \text{T}^{-1}$ and $\gamma_{\text{H}}/2\pi = 42.57 \text{ MHz} \cdot \text{T}^{-1}$, $v \approx 10^{-3} c$ and $\rho_{\text{DM}} \approx 0.4 \text{ GeV}/\text{cm}^3$. The full derivation of these expressions is given in S2.3 of the Supplementary Materials.

4.3. Signal processing

For each transient acquisition, the sample is prepared in the same initial state, which determines the phase of the J -coupling peaks. When averaging the transients together, the J -coupling peaks' amplitude and phase remain constant, while the uncorrelated noise is averaged away, thus increasing the SNR as the square root of the total integration time T_{tot} , i.e. $\text{SNR}(T_{\text{tot}}) \propto T_{\text{tot}}^{1/2}$.

However, the dark-matter-related information resides not in the J -coupling peaks, but in their sidebands. The external bosonic field oscillates at an unknown frequency and its phase at the beginning of each transient acquisition is unknown. This phase directly translates into the phase of the sidebands in the transient spectra: while the phase of the J -coupling peaks is identical from one transient acquisition to another, the phase of the sidebands varies. As a result, naively averaging the transient spectra averages the sidebands away, thus removing the dark-matter-related information from the resulting spectrum.

Here we use a post-processing phase-cycling technique which enables coherent averaging of the spectra in the frequency domain, even for transient signals for which no obvious experimental phase-locking can be achieved due to the unknown frequency of the signal. The method is similar to acquisition techniques in which an external clock is used to register the times of the transient acquisitions and post-processing phase shifting of the transient signals is employed to recover the external field's phase [48, 49].

The method relies on the fact that the bosonic field's phase at the beginning of each transient acquisition is unknown but not random. Indeed we recall that the bosonic fields remain phase coherent for $\sim 10^6$ oscillations, which for frequencies below 19 Hz is longer than the total integration time (14 hours). Thus, precise knowledge of the transient-signal acquisition starting times enables recovery of the phase of the bosonic field.

A full description of this averaging method is given in the Supplementary Materials S4. Each transient spectrum is incrementally phase-shifted prior to averaging. If the phase shift is equal to the phase accumulated by the bosonic field between two transient acquisitions, then the phase stability of the J -coupling peaks is shifted to their sidebands which can thus be coherently averaged.

Considering that the frequency of the bosonic field is unknown, the correct phase shift is also unknown. Thus, we repeat the operation for 2001 different phase increments between $[-\pi, \pi]$, yielding 2001 averaged spectra, one of which being averaged with the phase increment such that the sidebands are coherent.

To demonstrate the viability of this method, a small magnetic field was applied with amplitude 0.24 nT oscillating at 0.73 Hz, to simulate a dark-matter field. Using this processing technique, the SNR of the sidebands scales as $\text{SNR}(T_{\text{tot}}) \propto T_{\text{tot}}^{1/2}$ (see Fig. S4 in the Supplementary Materials), as expected during a coherent averaging procedure. This is a dramatic improvement over the alternative power-spectrum averaging (typically implemented for sets of incoherent spectra), which would yield a $T_{\text{tot}}^{1/4}$ scaling.

4.4. Calibration

The experimental sensitivity is defined by the ability to observe dark-matter-induced sidebands above the magnetometer noise floor. In order to show that the sideband amplitude scales with the modulation index, B/ω , and does not present unusual scalings due to experimental errors, two calibration experiments were performed. A first calibration was performed by varying the amplitude of the AC-field from 95 to 310 pT while holding the frequency constant at $\omega = 2\pi \times 0.73 \text{ Hz}$. Then the amplitude was held at 160 pT while varying the frequency, from 0.45 to 1.7 Hz. The results of this experiment are shown in Fig. S2 in the Supplementary Materials. Similar experiments were performed to determine the minimum detectable frequency (see S4 in the Supplementary Materials). Based on this calibration, we can extrapolate the expected sidebands amplitude, $A_s(B, \omega)$, for any field of amplitude B and frequency ω :

$$A_s(B, \omega) = 5.53 \times 10^{-6} \text{ rad} \cdot \text{s}^{-1} \times \frac{B[\text{T}]}{\omega[\text{rad} \cdot \text{s}^{-1}]}. \quad (16)$$

Then the magnetometer noise level determines the smallest detectable driving field, which is then converted to dark-matter coupling bounds via eqs. (12)-(15).

5. REFERENCES

References

- [1] L. Ackerman, M. Buckley, S. Carroll, and M. Kamionkowski. Dark matter and dark radiation. *Phys. Rev. D*, **79**, 023519, (2009).
- [2] G. Bertone and T. Tait. A new era in the search for dark matter. *Nature*, **562**, (2018).
- [3] G. Bertone, D. Hooper, and J. Silk. Particle dark matter: Evidence, candidates and constraints. *Phys. Rep.*, **405**, 279, (2005).
- [4] J. L. Feng. Dark matter candidates from particle physics and methods of detection. *Annu. Rev. Astron. Astr.*, **48**, 495, (2010).
- [5] P. W. Graham, I. G. Irastorza, S. K. Lamoreaux, A. Lindner, and K. A. van Bibber. Experimental searches for the axion and axion-like particles. *Annu. Rev. Nucl. Part. S.*, **65**, 485, (2015).
- [6] M. S. Safronova, D. Budker, D. DeMille, D. F. Jackson Kimball, A. Derevianko, and C. W. Clark. Search for new physics with atoms and molecules. *arXiv:1710.01833*, (2017).
- [7] R. Peccei and H. Quinn. CP conservation in the presence of pseudoparticles. *Phys. Rev. Lett.*, **38**, 1440, (1977).
- [8] P. Graham, D. Kaplan, and S. Rajendran. Cosmological relaxation of the electroweak scale. *Phys. Rev. Lett.*, **115**, 221801, (2015).
- [9] P. Svrcek and E. Witten. Axions in string theory. *J. High Energy Phys.*, **06**, 051, (2006).
- [10] S. J. Asztalos, G. Carosi, C. Hagmann, D. Kinion, K. van Bibber, M. Hotz, L. Rosenberg, G. Rybka, J. Hoskins, J. Hwang, P. Sikivie, D. B. Tanner, R. Bradley, and J. Clarke. SQUID-based microwave cavity search for dark-matter axions. *Phys. Rev. Lett.*, **104**, 1–4, (2010).
- [11] K. Zioutas, S. Andriamonje, V. Arsov, S. Aune, D. Autiero, F. Avignone, K. Barth, A. Belov, B. Beltran, H. Brauner, J. Carmona, S. Cebrian, E. Chesi, J. Collar, R. Creswick, T. Dafni, M. Davenport, L. Di Lella, C. Eleftheriadis, J. Englhauser, G. Fanourakis, H. Farach, E. Ferrer, H. Fischer, J. Franz, P. Friedrich, T. Gerasis, I. Giomataris, S. Gninenko, N. Golubev, M. Hasinoff, F. Heinsius, D. Hoffmann, I. Irastorza, J. Jacoby, D. Kang, K. Konigsmann, R. Kotthaus, M. Krüger, K. Kousouris, M. Kuster, B. Lakić, C. Lasseur, A. Liodios, A. Ljubicic, G. Lutz, G. Luzon, D. Miller, A. Morales, J. Morales, M. Mutterer, A. Nikolaidis, A. Ortiz, T. Papaevangelou, A. Placchi, G. Raffelt, J. Ruz, H. Riege, M. Sarsa, I. Savvidis, W. Serber, P. Serpico, Y. Semertzidis, L. Stewart, J. Vieira, J. Villar, L. Walckiers, K. Zachariadou, and C. Collaboration. First results from the CERN axion solar telescope. *Phys. Rev. Lett.*, **51**, (2005).
- [12] K. Ehret, M. Frede, S. Ghazaryan, M. Hildebrandt, E. Knabbe, D. Kracht, A. Lindner, J. List, T. Meier, N. Meyer, D. Notz, J. Redondo, A. Ringwald, G. Wiedemann, and B. Willke. Resonant laser power build-up in ALPS-A ‘light shining through a wall’ experiment. *Nucl. Instrum. Methods Phys. Res.*, **A 612**, 83–96, (2009).
- [13] R. Bradley, J. Clarke, D. Kinion, L. J. Rosenberg, K. van Bibber, S. Matsuki, M. Mück, and P. Sikivie. Microwave cavity searches for dark-matter axions. *Rev. Mod. Phys.*, **75**, 777, (2003).
- [14] B. M. Brubaker, L. Zhong, Y. V. Gurevich, S. B. Cahn, S. K. Lamoreaux, M. Simanovskaia, J. R. Root, S. M. Lewis, S. Al Kenany, K. M. Backes, I. Urdinaran, N. M. Rapidis, T. M. Shokair, K. A. van Bibber, D. A. Palken, M. Malnou, W. F. Kindel, M. A. Anil, K. W. Lehnert, and G. Carosi. First results from a microwave cavity axion search at 24 micro-eV. *Phys. Rev. Lett.*, **118**, 061302, (2017).
- [15] Y. Semertzidis. The axion dark matter search at CAPP: a comprehensive approach. *Bulletin of the American Physical Society*, (2017).
- [16] S. P. Experimental tests of the invisible axion phys. *Phys. Rev. Lett.*, **356**, (1983).
- [17] Y. Stadnik and V. Flambaum. Axion-induced effects in atoms, molecules, and nuclei: Parity nonconservation, anapole moments, electric dipole moments, and spin-gravity and spin-axion momentum couplings. *Phys. Rev. D*, **89**, 043522, (2014).
- [18] D. Budker, P. W. Graham, M. Ledbetter, S. Rajendran, and A. O. Sushkov. Proposal for a cosmic axion spin precession experiment (CASPER). *Phys. Rev. X*, **4**, 021030, (2014).
- [19] P. W. Graham and S. Rajendran. New observables for direct detection of axion dark matter. *Phys. Rev. D*, **88**, 035023, (2013).
- [20] D. F. Jackson Kimball, S. Afach, D. Aybas, J. W. Blanchard, D. Budker, G. Centers, M. Engler, N. L. Figueroa, A. Garcon, and P. W. Graham. Overview of the cosmic axion spin precession experiment (CASPER). *arXiv:1711.08999*, (2017).
- [21] T. Wang, D. F. Jackson Kimball, A. Sushkov, D. Aybas, J. Blanchard, G. Centers, S. O’ Kelley, A. Wickenbrock, J. Fang, and D. Budker. Application of spin-exchange relaxation-free magnetometry to the cosmic axion spin precession experiment. *Physics of the Dark Universe*, **19**, 27–35, (2018).
- [22] C. Abel, N. J. Ayres, G. Ban, G. Bison, K. Bodek, V. Bondar, M. Daum, M. Fairbairn, V. V. Flambaum, P. Geltenbort, K. Green, W. C. Griffith, M. van der Grinten, Z. D. Grujić, P. G. Harris, N. Hild, P. Iaydjiev, S. N. Ivanov, M. Kasprzak, Y. Kermaidic, K. Kirch, H.-C. Koch, S. Komposch, P. A. Koss, A. Kozela, J. Krempel, B. Lauss, T. Lefort, Y. Lemièrre, D. J. E. Marsh, P. Mohanmurthy, A. Mtchedlishvili, M. Musgrave, F. M. Piegsa, G. Pignol, M. Rawlik, D. Rebreyend, D. Ries, S. Rocca, D. Rozpedzik, P. Schmidt-Wellenburg, N. Severijns, D. Shiers, Y. V. Stadnik, A. Weis, E. Wursten, J. Zejma, and G. Zsigmond. Search for axionlike dark matter through nuclear spin precession in electric and magnetic fields. *Phys. Rev. X*, **7**, 041034, (2017).
- [23] J. Blanchard and D. Budker. Zero- to Ultralow-Field NMR. *eMagRes*, pages 1395–1410, (2016).
- [24] K. Blum and D. Kushnir. Neutrino signal of collapse-induced thermonuclear supernovae: The case for prompt black hole formation in SN 1987A. *The Astrophysical Journal*, **828**, 31, (2016).
- [25] J. Chang, R. Essig, and S. McDermott. Supernova 1987A constraints on sub-GeV dark sectors, millicharged particles, the QCD axion, and an axion-like particle. *arXiv:1803.00993*, (2018).
- [26] M. Vysotsky, Y. Zeldovich, M. Khlopov, and C. V.M. Some astrophysical limitations on the axion mass. *Journal of Experimental and Theoretical Physics Letters*, **27**, (1978).
- [27] J. Preskill, M. B. Wise, and F. Wilczek. Cosmology of the invisible axion. *Phys. Lett. B*, **120**, 127, (1983).
- [28] M. Dine and W. Fischler. The not-so-harmless axion. *Phys. Lett. B*, **120**, 137, (1983).
- [29] L. Abbott and P. Sikivie. A cosmological bound on the invisible axion. *Phys. Lett. B*, **120**, 133 – 136, (1983).
- [30] R. Catena and P. Ullio. A novel determination of the local dark matter density. *J. Cosmol. Astropart. P.*, **2010**, 004, (2010).
- [31] A. Nelson and J. Scholtz. Dark light, dark matter, and the misalignment mechanism. *Phys. Rev. D*, **84**, 103501, (2011).
- [32] M. Pospelov, S. Pustelny, M. P. Ledbetter, D. F. Jackson Kimball, W. Gawlik, and D. Budker. Detecting domain walls of axionlike models using terrestrial experiments. *Phys. Rev. Lett.*, **110**, 021803, (2013).
- [33] M. P. Ledbetter, T. Theis, J. W. Blanchard, H. Ring, P. Ganssle, S. Appelt, B. Blümich, A. Pines, and D. Budker. Near-zero-field nuclear magnetic resonance. *Phys. Rev. Lett.*, **107**, 107601, (2011).
- [34] G. Vasilakis, J. M. Brown, T. W. Kornack, and M. V. Romalis. Limits on new long range nuclear spin-dependent forces set with a $K-^3\text{He}$ comagnetometer. *Phys. Rev. Lett.*, **103**, 261801, (2009).

- [35] G. Raffelt. *Astrophysical Axion Bounds*. Springer Berlin Heidelberg, Berlin, Heidelberg, 2008.
- [36] T. Wu, J. W. Blanchard, G. P. Centers, N. L. Figueroa, A. Garcon, P. W. Graham, D. F. J. Kimball, S. Rajendran, Y. V. Stadnik, A. O. Sushkov, A. Wickenbrock, and D. Budker. Search for axionlike dark matter with nuclear spins in a single-component liquid. *arXiv:1901.10843*, (2019).
- [37] P. Graham, D. Kaplan, J. Mardon, S. Rajendran, W. Terrano, L. Trahms, and T. Wilkason. Spin precession experiments for light axionic dark matter. *Phys. Rev. D*, **97**, 055006, (2018).
- [38] R. W. Adams, J. A. Aguilar, K. D. Atkinson, M. J. Cowley, P. I. P. Elliott, S. B. Duckett, G. G. R. Green, I. G. Khazal, J. López-Serrano, and D. C. Williamson. Reversible interactions with para-hydrogen enhance NMR sensitivity by polarization transfer. *Science*, **323**, 1708–1711, (2009).
- [39] T. Theis, M. P. Ledbetter, G. Kervern, J. W. Blanchard, P. J. Ganssle, M. C. Butler, H. D. Shin, D. Budker, and A. Pines. Zero-field NMR enhanced by parahydrogen in reversible exchange. *J. Am. Chem. Soc.*, **134**, 3987–3990, (2012).
- [40] J.-B. Hövener, N. Schwaderlapp, T. Lickert, S. B. Duckett, R. E. Mewis, L. A. Highton, S. M. Kenny, G. G. Green, D. Leibfritz, J. G. Korvink, et al. A hyperpolarized equilibrium for magnetic resonance. *Nat. Commun.*, **4**, 2946, (2013).
- [41] M. Sufke, S. Lehmkuhl, A. Liebisch, B. Blümich, and S. Appelt. Para-hydrogen raser delivers sub-millihertz resolution in nuclear magnetic resonance. *Nat. Phys.*, **13**, 568, (2017).
- [42] A. Garcon, D. Aybas, J. W. Blanchard, G. Centers, N. L. Figueroa, P. W. Graham, D. F. J. Kimball, S. Rajendran, M. G. Sendra, A. O. Sushkov, L. Trahms, T. Wang, A. Wickenbrock, T. Wu, and D. Budker. The cosmic axion spin precession experiment (CASPER): a dark-matter search with nuclear magnetic resonance. *Quantum Science and Technology*, **3**, 014008, (2018).
- [43] T. Sjolander, M. Tayler, J. King, D. Budker, and A. Pines. Transition-Selective Pulses in Zero-Field Nuclear Magnetic Resonance. *J. Phys. Chem. A*, **120**, 4343–4348, (2016).
- [44] T. Wu, J. W. Blanchard, D. F. Jackson Kimball, M. Jiang, and D. Budker. Nuclear-spin comagnetometer based on a liquid of identical molecules. *Phys. Rev. Lett.*, **121**, 023202, (2018).
- [45] M. Jiang, T. Wu, J. W. Blanchard, G. Feng, X. Peng, and D. Budker. Experimental benchmarking of quantum control in zero-field nuclear magnetic resonance. *Sci. Adv.*, **4**, (2018).
- [46] M. C. D. Tayler, T. Theis, T. F. Sjolander, J. W. Blanchard, A. Kentner, S. Pustelny, A. Pines, and D. Budker. Invited review article: Instrumentation for nuclear magnetic resonance in zero and ultralow magnetic field. *Rev. Sci. Instrum.*, **88**, 091101, (2017).
- [47] K. A. Olive and M. Pospelov. Environmental dependence of masses and coupling constants. *Phys. Rev. D*, **77**, 043524, (2008).
- [48] B. Blümich, P. Blümli, and J. Jansen. Presentation of sideband envelopes by two-dimensional one-pulse (TOP) spectroscopy. *Solid State Nucl. Mag.*, **1**, 111 – 113, (1992).
- [49] S. Schmitt, T. Gefen, F. Stürner, T. Uden, G. Wolff, C. Müller, J. Scheuer, B. Naydenov, M. Markham, S. Pezzagna, J. Meijer, I. Schwarz, M. Plenio, A. Retzker, L. McGuinness, and F. Jelezko. Submillihertz magnetic spectroscopy performed with a nanoscale quantum sensor. *Science*, **356**, 832–837, (2017).

Acknowledgement: The authors would like to thank Dionysis Antypas, Deniz Aybas, Andrei Derevianko, Martin Engler, Pavel Fadeev, Matthew Lawson, Hector Masia Roig, and Joseph Smiga for useful discussions and comments. **Funding:** This project has received funding from the European Research Council (ERC) under the European Unions Horizon 2020 research and innovation programme (grant agreement No 695405). We acknowledge the support of the Simons and Heising-Simons Foundations and the DFG Reinhart Koselleck project. PWG acknowledges support from DOE Grant DE-SC0012012, NSF Grant PHY-1720397, DOE HEP QuantISED award #100495, and the Gordon and Betty Moore Foundation Grant GBMF794. DFJK acknowledges the support of

the U.S. National Science Foundation under grant number PHY-1707875. YVS was supported by the Humboldt Research Fellowship. **Authors contribution:** JWB, DB, DFJK and AOS conceived the project; JWB oversaw and managed the progress of the project; JWB and TW designed, constructed and calibrated the experimental apparatus and software controls. JWB, DB and AG conceived the data acquisition scheme; AG acquired and analysed the data with contribution of JWB, GC, NLF and TW; AG wrote the manuscript with the contribution of JWB, DB, GC, NLF, DFJK, AW and TW; PWG, DFJK, SR and YVS conceived the theory related to axion and hidden photon coupling to nuclear spins. All authors have read and contributed to the final form of the manuscript. **Competing interests:** the authors declare that they have no competing interests. **Data and materials availability:** all data needed to evaluate the conclusions in the paper are present in the paper and/or the Supplementary Materials. Additional data related to this paper may be requested from the authors.